DOI: 10.1002/ejic.200801248

Nitronyl Nitroxide Radicals Linked to Exchange-Coupled Metal Dimers – Studies Using X-ray Crystallography, Magnetic Susceptibility Measurements, EPR Spectroscopy, and DFT Calculations

Martin Jung,[a] Ajay Sharma,[b] Dariush Hinderberger,[b] Sebastian Braun,[c] Ulrich Schatzschneider,*[c] and Eva Rentschler*[a]

Keywords: Radicals / Nitronyl nitroxides / Magnetic properties / Density functional calculations

To study long-range magnetic interactions between exchange-coupled metal centers and a radical moiety coordinated through a peripheral group, three new homodimetallic complexes with Mn^{II}, Co^{II}, and Zn^{II} bridged by a nitronyl nitroxide (NIT) substituted benzoate ligand with the structure $[(NIT\text{-}C_6H_4\text{-}COO)M_2(L^R)](ClO_4)_2$ {M = Mn^{II}, Co^{II}, and Zn^{II}; NIT = nitronyl nitroxide and L^R = *N*,*N*,*N*′,*N*′-tetrakis(2-benzimidazolylalkyl)-2-hydroxy-1,3-diaminopropane} have been prepared and studied by X-ray crystallography, magnetic susceptibility measurements, EPR spectroscopy, and density functional theory calculations. For comparison, related complexes with Mn^{II} and Co^{II} bridged by a diamagnetic nitrobenzoate ligand were investigated by using the same methods. In all complexes, the metal centers have a trigonal-bipyramidal N_3O_2 coordination sphere, with the exception of the Mn^{II}-nitrobenzoate, where one of the two manganese centers is in a distorted octahedral environment due to the presence of an additional coordinated acetonitrile molecule. Magnetic susceptibility measurements on powdered samples revealed a dominant antiferromagnetic interaction between the metal ions. For the nitrobenzoate compounds, values of J_{Mn-Mn} = –5.8 cm^{-1} and J_{Co-Co} = –12.0 cm^{-1} are found. Replacement of the bridging ligand by a NIT-substituted benzoate group leads to very similar antiferromagnetic metal–metal interactions with J_{Mn-Mn} = –7.2 cm^{-1} and J_{Co-Co} = –12.0 cm^{-1}. A metal–radical interaction could not be observed. CW-X-band EPR measurements at low temperature show the anisotropic NIT signal. This confirms that the radical behaves like an isolated spin center and has no influence on the metal–metal interaction. These experimental data could be confirmed by DFT calculations at the UB3LYP level.

Introduction

Stable organic radicals are important building blocks for novel molecular magnetic materials. When coordinated to open-shell transition metals or lanthanides, they can help to overcome the problem of diminishing exchange interaction between the metal-centered spins, which is normally encountered in systems with an extended diamagnetic ligand framework. A large number of nitroxide, nitronyl nitroxide,[1–6] semiquinonate,[7–12] verdazyl,[13–16] thiazyl,[17–20] and other radicals are known to form discrete metal complexes as well as extended 1D, 2D, and 3D structures in the solid state, depending on the substitution pattern and presence of coligands.[21] Some of these systems exhibit interesting magnetic properties like the chain compound $[Co(hfac)_2NIT\text{-}C_6H_4O\text{-}R]_\infty$ recently reported by Ishida et al., which shows magnetic ordering below 4.5 K and a very large coercive field.[22,23] Usually, a close proximity between the metal center and the spin-bearing moiety of a radical is needed to ensure strong exchange interactions. To build extended 2D and 3D metal–radical structures, it is, however, necessary to introduce additional functionalities at the periphery of the radical ligands, and thus weak exchange interactions through such sites of low spin density need to be taken into account to fully rationalize the magnetic behavior of these systems.[24] In addition, long-range exchange interactions between radical centers and open-shell metal ions or clusters play an important role in enzymatic catalysis by a number of metalloenzymes.[25,26] The interaction between the $Y_Z^{\cdot}$ phenoxy radical and the water-oxidizing manganese cluster in photosystem II is probably the most prominent example, to mention just one.[27,28] Initial studies in this field from our group have focused on the coupling between a single paramagnetic metal ion and two functionalized NIT radical ligands coordinated through peripheral

[a] Institut für Anorganische Chemie und Analytische Chemie, Johannes Gutenberg-Universität Mainz, Duesbergweg 10–14, 55128 Mainz, Germany
Fax: +49-6131-39-23922
E-mail: rentschler@uni-mainz.de
[b] Max-Planck-Institut für Polymerforschung, Ackermannweg 10, 55128 Mainz, Germany
[c] Lehrstuhl für Anorganische Chemie I – Bioanorganische Chemie, Ruhr-Universität Bochum NC 3/74, Universitätsstr. 150, 44801 Bochum, Germany
Fax: +49-234-32-14378
E-Mail: ulrich.schatzschneider@rub.de
Supporting information for this article is available on the WWW under http://www.eurjic.org/ or from the author.

phenolate groups.[24] To investigate the inverse situation, the competitive coupling between two metal centers and a single radical ligand through an alternative carboxylate linker, we have now prepared homodimetallic manganese(II), cobalt(II), and zinc(II) complexes held together by the chelating ligand *N*,*N*,*N*′,*N*′-tetrakis(2-benzimidazolylalkyl)-2-hydroxy-1,3-diaminopropane, with the two metal centers additionally bridged by a NIT-substituted benzoate group through the peripheral carboxyl group. The series of compounds prepared was fully characterized by methods including X-ray crystallography for all compounds to allow a correlation of their magnetic properties with the molecular structure. Magnetic susceptibility measurements were complemented by DFT calculations to allow a complete understanding of the exchange interaction pathways present in these molecules.[29] In addition, model compounds in which nitrobenzoate serves as a diamagnetic substitute of the NIT benzoic acid were prepared to study the metal–metal exchange interaction.

Results and Discussion

Dinuclear manganese(II), cobalt(II), and zinc(II) complexes **1**, **2**, and **3** chelated by deprotonated ligand *N*,*N*,*N*′,*N*′-tetrakis(*N*-propyl-2-benzimidazolyl)-2-hydroxy-1,3-diaminopropane (L^{nPr}) and bridging NIT-C_6H_4-COO^- were prepared by mixing the constituents in methanol followed by recrystallization of the precipitated crude product from acetonitrile/diethyl ether.

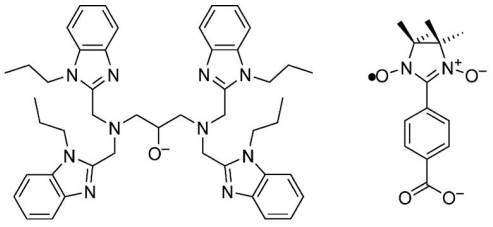

$[L^{nPr}]^-$ $[NIT\text{-}C_6H_4\text{-}COO]^-$

Complexes **4** and **5**, in which the nitrobenzoate serves as a diamagnetic substitute of the NIT benzoic acid, were prepared in a similar way as **1**, **2** and **3** to study the metal–metal exchange interaction. All five complexes gave satisfactory elemental analyses and could be characterized by X-ray crystallography. Relevant data for compounds containing the NIT radical are collected in Table 2.

Crystal and Molecular Structure of $[Mn_2(L^{nPr})(O_2CPhNIT)](ClO_4)_2\cdot Et_2O\cdot 1.5H_2O$ (1)

Complex **1** with the NIT-substituted benzoate ligand features two pentacoordinate Mn^{II} centers with a N_3O_2 ligand set each (Figure 1). Both metals have a trigonal-bipyramidal coordination environment, with τ values[30] of 0.89 and 1.00 for Mn(1) and Mn(2), respectively. The six-membered ring formed by the two manganese(II) ions, the alkoxide oxygen atom, and the three atoms of the carboxylate group has a boat conformation, in which Mn(1), O(1), O(3), and C(48) are essentially coplanar, while Mn(2) and O(2) are above the plane by 0.237 and 0.174 Å, respectively. The phenyl ring of the NIT ligand is tilted relative to the carboxylate group by an angle of 24.0°, which is comparable to the other compounds. All parameters of the imidazolidine ring are close to those of other NIT radicals and virtually identical to those of the free ligand. The tilt angle between the phenyl ring and the mean plane of the NIT group is 46.2°, which compares well to the values found for other NIT benzoate complexes.[28,31,32]

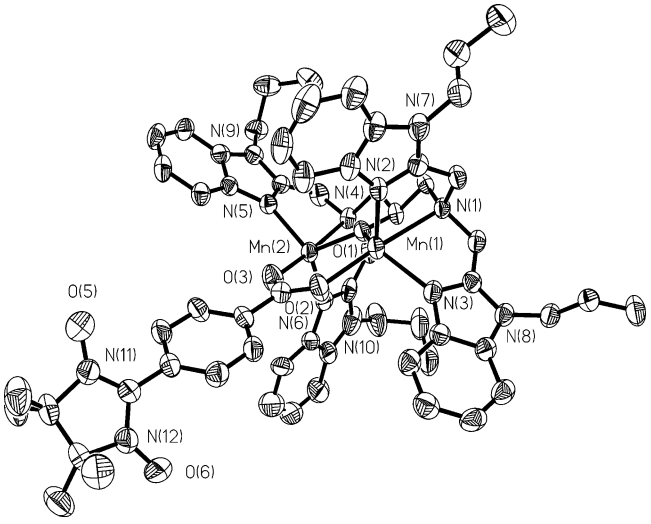

Figure 1. Molecular structure of **1**; counterions, hydrogen atoms and solvate water, as well as diethyl ether molecules, are not shown. Ellipsoids are drawn at the 50% probability level.

For an interpretation of the magnetic susceptibility measurements carried out on solid samples, it is important to check for close intermolecular contacts between the spin-bearing moieties. While the two manganese ions are well isolated from neighboring molecules buried in the L^{nPr} binding pocket, both N–O groups from the NIT moiety show some notable intermolecular contacts. First of all, there is an antiparallel arrangement of O(5)–N(11) and O(5B)–N(11B) with two identical intermolecular N···O distances of 4.292 Å (B = $-x$, $-y + 1$, $-z$). In addition, O(6) shows close contacts to H(2aC) and H(3bC) from the 2-hydroxypropane-1,3-diamine group of a neighboring molecule at 2.585 and 2.473 Å, respectively (C = $x - 1$, x, z). Though the former contact is between NIT N–O groups, which carry considerable spin density,[32] the distance is too long to give rise to a notable intermolecular exchange interaction.[33] The latter, on the other hand, is close, but the alkyl backbone of the L^{nPr} ligand is not expected to bear any significant spin density. Thus, the molecules can be considered as magnetically isolated in the solid state.

Crystal and Molecular Structure of $[Co_2(L^{nPr})(O_2CPhNIT)](ClO_4)_2\cdot 0.5Et_2O$ (2)

Cobalt complex **2** has a structure bearing great similarity to that of manganese compound **1** (see Supporting Infor-

mation). The two cobalt(II) centers have a trigonal-bipyramidal coordination environment with τ = 0.92 for Co(1) and τ = 0.97 for Co(2), which is smaller than that in complex **1**. The Co(1)–O(1)–Co(2) angle, which is important for interpretation of the magnetic susceptibility data, is 126.0(3)° and thus slightly larger than that in manganese compound **1**. Both carboxylate oxygen atoms and the amine nitrogen atoms from L^{nPr} are in the apical positions of the trigonal bipyramid, as in the other compounds. The phenyl ring is tilted relative to the carboxylate group by an angle of 21.5°, which is comparable to the other compounds. The tilt angle between the phenyl ring and the mean plane of the NIT group is 45.1° and thus essentially identical to that in manganese complex **1**. Short intermolecular contacts between spin-bearing moieties are also absent in **2**. The closest distances (< 3 Å) of the NO groups from the NIT involve only the diamagnetic ligand framework. Thus, the complex can be considered as magnetically isolated in the solid state.

Crystal and Molecular Structure of $[Zn_2(L^{nPr})(O_2CPhNIT)](ClO_4)_2 \cdot Et_2O \cdot 1.5H_2O$ (3)

In zinc compound **3**, both metal centers also have a trigonal-bipyramidal coordination geometry, although it deviates a little more from the ideal value for Zn(1) with τ = 0.86 relative to that for Zn(2) with τ = 0.97, which is similar to the deviation in complex **1**. The Zn(1)–O(1)–Zn(2) angle is 124.4(5)°, which is essentially identical to that found for the other four complexes (see Supporting Information). The rest of the structure is also very similar to those of the other two NIT compounds. At 18.9°, the tilt between the coordinated carboxylate and the phenyl ring is a little smaller, but the phenyl–imidazolidine angle of 42.1° is in the range expected for NIT compounds. No close intermolecular contacts between the paramagnetic NIT groups are found in this compound. In addition to **1**, **2**, and **3**, incorporating a bridging paramagnetic NIT-$PhCOO^-$ nitrobenzoate, the manganese(II) and cobalt(II) complexes **4** and **5** with a diamagnetic nitrobenzoate ligand could be crystallized. Information on the data collection and structural refinement is given in Table 3.

Crystal and Molecular Structure of $[Mn_2(L^{nPr})(O_2CPhNO_2)(CH_3CN)](ClO_4)_2$ (4)

Manganese complex **4** shows the expected binding mode of ligand L^{nPr}, in which each of the metal centers is coordinated by a tertiary amine nitrogen and two benzimidazole groups (Figure 2). In addition, the Mn^{II} atoms are bridged by the alkoxide group from L^{nPr} and the carboxylate moiety of the nitrobenzoate. However, while Mn(1) is in a N_3O_2 coordination environment, an additional acetonitrile molecule is bound to Mn(2), which thus has a N_4O_2 ligand sphere. With an O(2)–Mn(1)–N(4) angle of 179.34(12)° and τ = 1.01, the pentacoordinate Mn(1) is in an almost perfect trigonal-bipyramidal coordination mode, in which the trigonal is plane formed by O(1), N(5), and N(6). In contrast, Mn(2) has a significantly distorted octahedral ligand environment, in which especially the O(1)–Mn(2)–N(2) angle is compressed to only 144.93(12)° while N(3)–Mn(2)–N(12) and O(3)–Mn(2)–N(1) are somewhat closer to linearity at 169.60(13)° and 167.56(12)°, respectively. Thus, the coordination sphere of one manganese ion is different from that in manganese complex **1**, which can be explained by packing effects and is also known from studies on similar complexes.[34] The two manganese(II) ions, the alkoxide oxygen, and the three atoms of the carboxylate group form a six-membered ring with a boat conformation, in which O(1), Mn(2), O(2), and C(48) are essentially coplanar while both Mn(1) and O(3) are located above the mean plane at 0.606 and 0.203 Å, respectively. The Mn(1)–O(1)–Mn(2) angle is 116.71(12)°. While the nitro group is essentially coplanar with the phenyl ring, the latter is tilted relative to the carboxylate group by 24.8°.

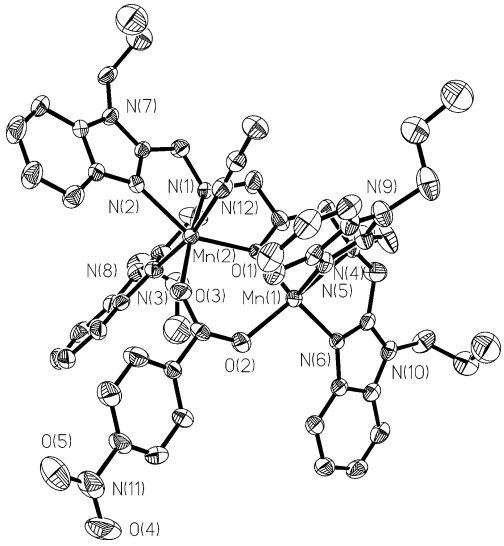

Figure 2. Molecular structure of **4**; counterions and hydrogen atoms are not shown. Ellipsoids are drawn at the 50% probability level.

Crystal and Molecular Structure of $[Co_2(L^{nPr})(O_2CPhNO_2)](PF_6)_2$ (5)

In cobalt complex **5**, ligand L^{nPr} shows a similar binding mode, but both metal centers are now in a pentacoordinate N_3O_2 ligand environment (Figure 3). With τ values of 0.99 and 0.97 for Co(1) and Co(2), respectively, both cobalt ions have an almost perfect trigonal-bipyramidal coordination sphere in which the axis perpendicular to the trigonal plane points from the carboxylate oxygen atom towards the amine nitrogen of L^{nPr}, as in the related manganese complex, but the Co(1)–O(1)–Co(2) angle of 122.47(10)° is a little larger, but very close to that in manganese NIT complex **1**. The two cobalt(II) ions, the alkoxide oxygen, and the three atoms of the carboxylate group also form a six-membered ring, but now with an envelope conformation, in which Co(1) and Co(2) as well as O(1) and O(2) are coplanar,

while O(3) and C(48) are above the plane by 0.609 and 0.385 Å, respectively. In the cobalt complex, the phenyl ring is also tilted relative to the carboxylate group, although the angle, at 21.9°, is slightly smaller.

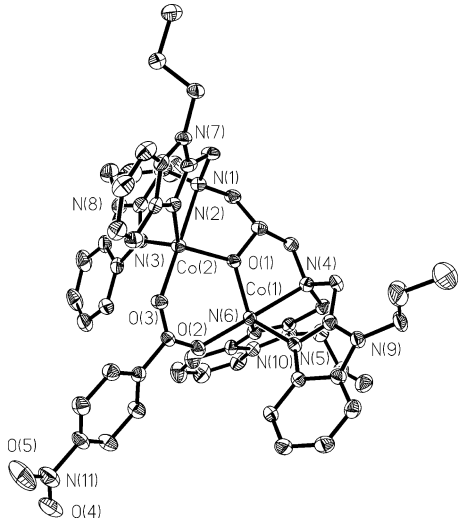

Figure 3. Molecular structure of **5**; counterions and hydrogen atoms are not shown. Ellipsoids are drawn at the 50% probability level.

Magnetic Properties of the Complexes

For the determination of the exchange coupling between the two metal ions without interference from the NIT radical, the temperature dependence of the molar magnetic susceptibility for **4** and **5** was measured in the temperature range 2 to 300 K. The $\chi_m T$ values steadily decrease upon lowering the temperature for both **4** and **5** from 4.23 and 7.24 $cm^3 K mol^{-1}$ respectively at 300 K to zero at the lowest attainable temperature of 2 K (Figure 4). This is indicative of a strong intramolecular antiferromagnetic exchange interaction. The temperature dependence of the molar magnetic susceptibility was modeled by using a fitting procedure to the appropriate Heisenberg–Dirac–Van Vleck (HDVV) spin Hamiltonian[35,36] for isotropic exchange coupling [Equation (1)].[37]

$$\hat{H} = -2J'\hat{S}_{M1}\hat{S}_{M2} \quad (1)$$

A reasonable fit was obtained for the dimanganese complex **4** with $g_{Mn} = 2.0$, which is expected for manganese(II) ions in the high-spin $S = 5/2$ state, where contributions from the angular momentum are absent. The exchange parameter was determined as $J_{Mn-Mn} = -5.8\ cm^{-1}$. For dicobalt compound **5**, a reasonable fit was obtained with the following parameters: $g_{Co} = 2.3$, $J_{Co-Co} = -12.0\ cm^{-1}$ (Table 1).

Table 1. Comparison of experimental and calculated exchange coupling parameters J and J' for compounds **1**, **2**, **4**, and **5**.

Compound	J_{exp} /cm^{-1}	J'_{exp} /cm^{-1}	J_{calc} /cm^{-1}	J'_{calc} /cm^{-1}
Mn-Mn-NIT **1**	0.0 (fixed)	–7.2	+1.9	–10.1
Co-Co-NIT **2**	0.0 (fixed)	–12.0	–0.1	–15.4
Mn-Mn **4**	–	–5.8	–	–10.1
Co-Co **5**	–	–12.0	–	–15.4

Plots of the molar magnetic susceptibility vs. temperature for the metal–radical complexes **1** to **3** are shown in Figure 5. The $\chi_m T$ values of **1** and **2** steadily decrease upon lowering the temperature to a value of 0.35 $cm^3 K mol^{-1}$ at 2 K, which corresponds to the spin-only value of an isolated unpaired electron. The $\chi_m T$ vs. T plot for complex **1** was simulated by using the following parameters: $g_{Mn} = g_{NIT} = 2.0$ and $J_{Mn-Mn} = -7.2\ cm^{-1}$, while the metal–radical exchange interaction was fixed at zero. This assumption differs from a previous study,[28] in which a weak antiferromagnetic interaction of $-1(\pm 1)\ cm^{-1}$ was extracted from the temperature magnetic data for the coupling between the NIT radical and a mixed-valent $Mn^{III/IV}$ dimer bearing a spin ground state different from zero. For complex **2**, similar results were obtained with $g_{Co} = 2.3$, $g_{NIT} = 2.0$, and $J_{Co-Co} = -12.0\ cm^{-1}$. Also here, J_{Co-NIT} was set to zero. In the case of zinc(II) complex **5**, the expected paramagnetic behavior of NIT in the absence of intermolecular exchange interactions was observed (Figure 5).

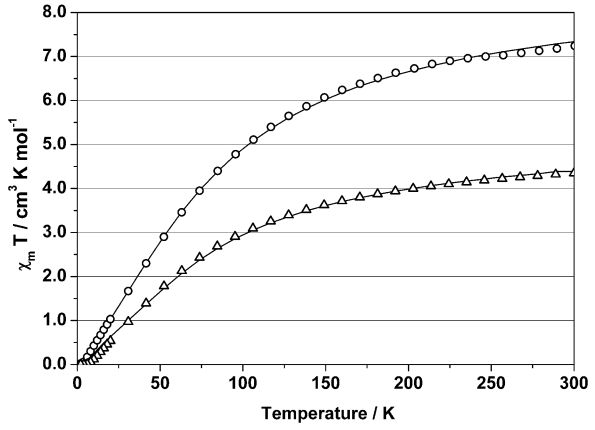

Figure 4. Temperature dependence of the molar magnetic susceptibility for **4** (○) and **5** (Δ); solid lines: simulation of the experimental data, see text for parameters.

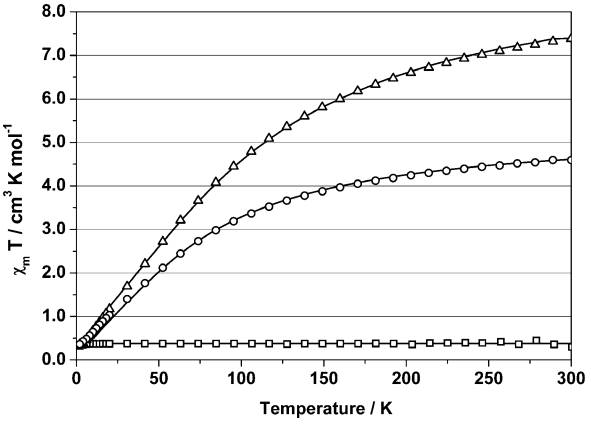

Figure 5. Temperature dependence of the molar magnetic susceptibility for **1** (Δ), **2** (○), and **3** (□); solid line: simulation of the experimental data, see text for parameters.

EPR Spectroscopy

At high temperature, no signal assignable to the metal centers was observed. For **1**–**3** the data at 10 K show the anisotropic signal typical for the NIT radical (Figure 6). The EPR signal of **2** is broader and can be simulated with the same *g* and *A* parameters (see Supporting Information).

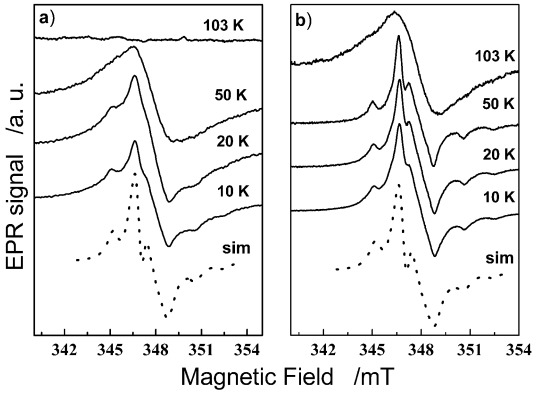

Figure 6. Temperature dependence of the CW-X-band EPR signal of a solution of (a) **1** and (b) **3** [2 mmol in acetonitrile/toluene (1:1) for 10, 20, and 50 K; 2 mmol in acetonitrile for 103 K]. The solid lines represent the experimental data at various temperatures. The dotted line represents the simulation of the spectra ($g_\perp$ = 2.0095, $g_\parallel$ = 2.0015; $A_\perp$ = –0.45 mT, $A_\parallel$ = 1.75 mT).

The absence of metal signals in all EPR spectra is the direct consequence of the antiferromagnetic coupling between the metal ions. This exchange coupling causes a fast relaxation of the excited states and could not be avoided by cooling to very low temperatures, since at low temperature the metal dimer populates a diamagnetic ground state, as observed also by magnetic susceptibility measurements for **4** and **5**. The non-zero spin ground state of **1**–**3**, as observed by magnetic measurements, could be identified by EPR spectroscopy as $S = 1/2$, which is almost exclusively located on the NIT moiety and not on the metal ions. The hyperfine pattern of **1** to **3** proves that the unpaired electron is still located in the π* MO of the N–O bonds. The angular momentum operator in *z* direction, L_Z, causes an additional spin–orbital contribution for $g_X = g_Y = g_\perp$, but not for $g_Z = g_\parallel$, which leads to the observed values $g_\perp > g_\parallel \approx g_e$. The spin density in the singly occupied molecular orbital has also a stronger interaction with the nuclear spin of the nitrogen atom in the *z* direction than that in the *xy* direction, which leads to $A_\perp < A_\parallel$.

Density Functional Calculations

To verify the exchange coupling parameters determined from the fitting of the magnetic susceptibility data, we carried out density functional theory calculations of the energies of the different spin states of compounds **1**, **2**, **4**, and **5** at the UB3LYP level. By using the coordinates from the X-ray structure determinations without any geometric relaxation and very strict convergence, semiquantitative results can be obtained. For the nitrobenzoate complexes **4** and **5**, both the high-spin (HS) and the broken-symmetry (BS) open-shell singlet states were converged. In both NIT compounds **1** and **2**, a total of four spin states were studied for each molecule: (a) all spins parallel, (b) the spin of the organic radical moiety antiparallel to the ferromagnetically coupled dimetal unit, and (c) two states in which the metals are antiferromagnetically coupled and the radical spin is parallel to one or the other metal center. These latter two states were found to be nearly degenerate, and thus these systems were treated as symmetrical triangular by using the Hamiltonian

$$\hat{H} = -2J(\hat{S}_{M1}\hat{S}_{rad} + \hat{S}_{M2}\hat{S}_{rad}) - 2J'(\hat{S}_{M1}\cdot\hat{S}_{M2})$$

with

$$\hat{S}' = \hat{S}_{M1} + \hat{S}_{M2}$$

and

$$\hat{S} = \hat{S}' + \hat{S}_{rad}$$

one then obtains for the energies of the spin states in zero field

$$E(S,S') = -JS(S + 1) - (J' - J)S'(S' + 1).$$

For the manganese(II) radical system, the relative energies of the states thus are

$E(1/2, 0) = -6J + 30J'$
$E(9/2, 5) = 0$
$E(11/2, 5) = -11J.$

The corresponding expression for the related cobalt(II) radical compound is

$E(1/2, 0) = -4J + 12J'$
$E(5/2, 3) = 0$
$E(7/2, 3) = -7J.$

All states could be converged starting from the electron density of the high-spin state and gave spin density distributions in accordance with the expected open-shell HS or BS states. Calculated exchange coupling parameters *J* and *J'* are compared to the experimental ones in Table 1.

With a mean deviation of 3.5 cm^{-1} between the experimental and calculated exchange parameters *J'*, there is semiquantitative agreement between the susceptibility measurements and the DFT calculations. Although the sign is correctly reproduced in all cases, DFT overestimates the absolute values by 130 to 170%. The calculated metal–radical couplings of $|J| < 2$ cm^{-1} are too small to be determined by susceptibility measurements and thus have not been included in the fit to the experimental data. Nonetheless the DFT calculations show that a weak long-range spin-exchange interaction between the NIT radical and the metal ions is still possible.

Conclusions

Three new homometallic manganese(II), cobalt(II), and zinc(II) complexes, with the dimetallic center each bridged by a NIT-substituted benzoate, have been synthesized and fully characterized by methods including X-ray structure

determinations for all compounds. In addition, the related Mn and Co complexes with a diamagnetic nitrobenzoate ligand have been prepared and characterized. In the solid-state structures, no significant short intermolecular contacts were found, and thus the compounds can be considered as also magnetically isolated. The susceptibility measurements show dominant antiferromagnetic interactions in the metal–radical compounds that can be attributed to a spin exchange only within the dimetallic unit. Evidenced by comparison with the analogous nitrobenzoate-bridged manganese(II) and cobalt(II) model compounds no metal–radical interaction could be observed. EPR measurements support the observation that the spin ground state has only radical character, as indicated by the anisotropic signal of NIT. No exchange between the ONCNO group and the paramagnetic metal ions over the benzoate group is observed, as in principle would be possible by the interaction of the π* orbital with the delocalized π system of the phenylene ring through the spin-polarization mechanism. In fact, only small contributions to the magnetic interaction would be expected through the carbon substituent, since NIT bears a nodal plane on the carbon atom linking the substituent. Experimental data show that the NIT here behaves as an isolated spin center of $S = 1/2$, which could be further confirmed by DFT calculations. In summary the coordination of the NIT-benzoate ligand to a antiferromagnetically coupled homometallic metal dimer only leads to a shift of the spin ground state but has no observable effect on the exchange interaction. In order to observe a radical–metal interaction, it is necessary to synthesize coordination compounds in which high-spin ground states are populated. This could be achieved, for example, in heterometallic or mixed-valence systems or ferromagnetically coupled metal dimers.

Experimental Section

General: All chemicals were reagent grade and used as received without further purification. C, H, and N analysis was performed with a Foss Heraeus Vario EL elemental analyzer. Molecular weights and formulas were calculated without solvent molecules unless explicitly stated.

Spectroscopy: CW-X-band EPR spectra in the temperature range 10 to 100 K were recorded with a Bruker Elexsys 580 cw/pulse EPR spectrometer (ν = 9.772 GHz) having a dielectric resonator (MD4EN, overcoupled to Q values of typically 100). The temperature was controlled by cooling with liquid helium by using an Oxford cryostat and cooling system. The measurements above 100 K were measured with a Magnettech Miniscope MS200 benchtop CW EPR spectrometer (ν = 9.335 GHz), with a variable-temperature cooling/heating finger. The EPR parameters were obtained from spectral simulations by using the program package Easyspin 2.7.1.[38,39] NMR spectra were recorded by using a Bruker DRX 400 spectrometer. Infrared spectra were recorded in the 400–4000 cm^{-1} range with a Jasco FT/IR-4200 spectrometer. The IR measurements were carried out by using the pellet technique with KBr as embedding medium.

Synthesis of Ligand HL^{nPr}: The ligand was synthesized according to a published method.[40] 1,3-Diamino-2-hydroxypropane-*N*,*N*,*N*′,*N*′-tetraacetic acid (43.0 g, 0.14 mol) and 1,2-diaminobenzene (60.7 g, 0.56 mol) were suspended in ethylene glycol (250 mL) and heated to 180 to 190 °C for 3 h. After being cooled to room temperature, the solution was poured into water (2 L), leading to the formation of a light blue precipitate. The water was decanted, and the remaining solid was washed with hot acetone (2 × 250 mL). The product was then collected by filtration to obtain *N*,*N*,*N*′,*N*′-tetrakis[(2-benzimidazolyl)methyl]-1,3-diaminopropane (HL) as a light blue solid (48.5 g, 57% yield). This product was immediately used without characterization in the following alkylation, which was performed according to a method described in the literature.[41] Thus, *N*,*N*,*N*′,*N*′-tetrakis[(2-benzimidazolyl)methyl]-1,3-diaminopropane (48.5 g, 0.08 mol) was added to a suspension of powdered potassium hydroxide (60.0 g) in dimethyl sulfoxide (300 mL). Then, 1-bromopropane (59.0 g, 0.48 mol) was added, and the mixture was stirred for 1 h at room temperature. Afterwards, the reaction mixture was poured into water (2 L), leading to the formation of a precipitate. The water was decanted, and the precipitate was redissolved in chloroform (250 mL). The organic layer was separated, washed with water (2 × 100 mL), and then dried with magnesium sulfate. The solvent was removed under reduced pressure to give *N*,*N*,*N*′,*N*′-tetrakis[(1-*n*-propylbenzimidazol-2-yl)methyl]-1,3-diaminopropane (HL^{nPr}) as a beige solid (54.1 g, 85% yield). ^1H NMR ($CDCl_3$): δ = 0.62 (t, 3 H), 1.50 (q, 4 H), 2.65 (m, 4 H), 3.72 (m, 1 H), 3.90 (q, 8 H), 4.00 (dd, 8 H) 7.18 (m, 12 H), 7.66 (m, 4 H) ppm. ^{13}C NMR ($CDCl_3$): δ = 10.9, 22.7, 44.7 51.8, 59.9, 68.7, 109.5, 119.2, 121.7, 122.3, 135.1, 142.0, 151.5 ppm. IR: $\tilde{\nu}$ = 3410 (sh) m, 3052 (m), 2963 (m), 2931 (m), 2839 (m), 1614 (w), 1510 (m), 1481 (s), 1418 (s), 1361 (m), 1331 (s), 1286 (m), 1250 (w), 1115 (m), 1061, 768 (w), 741 (s) cm^{-1}. FD-MS: m/z = 778.5 [M^+].

Synthesis of NIT-PhCOOH and Its Sodium Salt: NIT-C_6H_4-COOH was prepared according to the literature.[42] To convert the NIT-benzoic acid to the sodium salt, NIT-PhCOOH (10.0 g, 36 mmol) was suspended in water (200 mL). Then, sodium hydroxide (1.4 g, 35 mmol) was added, and the mixture was stirred until a clear blue solution was obtained. The water was then removed under reduced pressure to give a blue solid. This was washed with acetonitrile, filtered, and dried in air, to give NIT-C_6H_4-COONa (10 g, 92% yield).

Synthesis of the Metal Complexes

$[Mn_2(L^{nPr})(O_2CPhNIT)](ClO_4)_2\cdot Et_2O\cdot 1.5H_2O$ (1): HL^{nPr} (0.78 g, 1.0 mmol) was dissolved in methanol (40 mL), and then a methanol solution of manganese(II) perchlorate hexahydrate (0.75 g, 2.0 mmol) was added while stirring at room temperature until a slurry appeared. Then, NIT-C_6H_4-COONa (0.4 g, 1.5 mmol) was added as a solid, and the resulting suspension was stirred at room temperature for 1 h. The blue precipitate formed was filtered off and dried in air. The crude product was dissolved in acetonitrile and filtered again. Vapor diffusion of diethyl ether into an acetonitrile solution gave 1.06 g (73% yield) dark blue-green crystals of **1**. $C_{61}H_{73}Cl_2Mn_2N_{12}O_{13} + Et_2O + H_2O$ (1455.22): calcd. C 53.65, H 5.89, N 11.55; found C 53.76, H 5.33, N 11.63. IR: $\tilde{\nu}$ = 3458 (sh) m, 3080 (vw), 2988 (w), 2935 (w), 2877 (w), 1589 (m), 1544 (m), 1486 (m), 1453 (m), 1407 (m), 1361 (m), 1293 (m), 1255 (m), 1092 (s), 982 (w), 939 (w), 898 (w), 748 (m), 622 (m), 507 (vw), 437 (vw) cm^{-1}. ESI-MS: m/z = 1262.2 [$M - ClO_4^-$], 581.8 [$M - 2ClO_4^-$]

$[Co_2(L^{nPr})(O_2CPhNIT)](ClO_4)_2\cdot 0.5Et_2O$ (2): This complex was prepared in the same way as **1** by using NIT-C_6H_4-COONa (0.4 g, 1.5 mmol). Vapor diffusion of diethyl ether into the acetonitrile solution gave 1.11 g (79% yield) violet crystals of **2**. $C_{61}H_{73}Cl_2Co_2N_{12}O_{13} + 2H_2O$ (1407.11): calcd. C 52.07, H 5.52, N 11.95; found C 51.91, H 5.43, N 12.03. IR: $\tilde{\nu}$ = 3427 (sh) m, 2966

(w), 2931 (w), 2877 (w), 1589 (m), 1548 (m), 1493 (m), 1454 (m), 1404 (m), 1293 (m), 1084 (s), 980 (w), 943 (w), 900 (w), 747 (m), 624 (m), 527 (vw), 436 (vw) cm^{-1}. ESI-MS: *m*/*z* = 1270.2 [M – ClO_4^-], 585.8 [M – $2ClO_4^-$]

[$Zn_2(L^{nPr})(O_2CPhNIT)](ClO_4)_2·0.5Et_2O·1.5H_2O$ (3): This complex was prepared in the same way as **1** by using NIT-C_6H_4-COONa (0.4 g, 1.5 mmol). Vapor diffusion of diethyl ether into the acetonitrile solution gave 1.16 g (78% yield) blue-green crystals of **3**. $C_{61}H_{73}Cl_2N_{12}O_{13}Zn_2 + 2H_2O$ (1420.02): calcd. C 51.59, H 5.47, N 11.84; found C 51.73, H 5.26, N 11.97. IR: ṽ = 3470 (sh) m, 2965 (w), 2932 (w), 2876 (w), 1591 (m), 1549 (m), 1496 (m), 1455 (m), 1407 (m), 1361 (m), 1293 (m), 1090 (s), 943 (w), 898 (w), 748 (m), 623 (m), 439 (vw) cm^{-1}. ESI-MS: *m*/*z* = 1284.2 [M – ClO_4^-], 592.8 [M – $2ClO_4^-$]

[$Mn_2(L^{nPr})(O_2CPhNO_2)(CH_3CN)](ClO_4)_2$ (4): HL^{nPr} (0.78 g, 1.0 mmol) was dissolved in methanol (40 mL), and then a methanol solution of manganese(II) perchlorate hexahydrate (0.75 g, 2.0 mmol) was added while stirring at room temperature until a slurry appeared. Then, sodium nitrobenzoate (0.28 g, 1.5 mmol) was added as a solid, and the resulting suspension was stirred at room temperature for 1 h. The white precipitate formed was filtered off and dried in air. The crude product was dissolved in acetonitrile and filtered again. Vapor diffusion of diethyl ether into an acetonitrile solution gave 1.07 g (83% yield) light beige crystals of **4**. $C_{54}H_{61}Cl_2Mn_2N_{11}O_{13} + 2H_2O$ (1420.02): calcd. C 51.77, H 4.91, N 12.30; found C 51.51, H 4.78, N 12.10. IR: ṽ = 3440 (sh) m, 3059 (vw), 2980 (w), 2938 (w), 2879 (w), 1576 (m), 1486 (m), 1453 (m), 1413 (m), 1344 (m), 1088 (s), 938 (w), 899 (w), 748 (m), 622 (m), 520 (w) cm^{-1}. ESI-MS: *m*/*z* = 1152.2 [M – CH_3CN – ClO_4^-], 526.98 [M – $2ClO_4^-$]

[$Co_2(L^{nPr})(O_2CPhNO_2)](PF_6)_2$ (5): HL^{nPr} (0.78 g, 1.0 mmol) was dissolved in methanol (40 mL), and then a methanol solution of cobalt(II) chloride hexahydrate (0.5 g, 2.1 mmol) was added while stirring at room temperature until a slurry appeared. Then, sodium nitrobenzoate (0.28 g, 1.5 mmol) and sodium hexafluorophosphate (0.69 g, 4 mmol) were added in solid form, and the suspension was stirred at room temperature for 1 h. The violet precipitate formed was filtered and dried in air. The crude product was dissolved in acetonitrile and filtered again. Vapor diffusion of diethyl ether into the acetonitrile solution gave 1.16 g (86% yield) violet crystals of **5**. $C_{54}H_{61}Co_2F_{12}N_{11}O_5P_2$ (1351.93): calcd. C 52.07, H 5.52, N 11.95; found C 48.16, H 4.71, N 11.53. IR: ṽ = 3434 (sh) m, 2970 (w), 2938 (w), 2889 (w), 1569 (m), 1493 (m), 1454 (m), 1408 (m), 1348 (m), 944 (w), 841 (s), 748 (m), 557 (m), 529 (w) cm^{-1}. ESI-MS: *m*/*z* = 1206.0 [M – PF_6^-], 530.9 [M – $2PF_6^-$]

Computational Details: All calculations were carried out as single-point runs by using the coordinates available from the X-ray structure determinations with ORCA 2.6.35 on a Dell Optiplex 745 computer running Ubuntu 4.2.3 as the operating system.[43] Counterions and solvate molecules were removed to only treat the cationic unit. Alkyl substituents on the benzimidazolyl groups were truncated to methyl groups, the hydrogen atom being placed along the original C–C axis at an average distance. The unrestricted B3LYP functional was used in the calculation of the spin density distribution and energies, with a TZVP basis set on the metal and radical centers as well as the donor atoms directly coordinated to the metal.[44] For all other atoms, a DZ(P) basis was employed.[45] Because of the very small energy differences expected, a very tight convergence criterion (option VeryTightSCF, energy change *TolE* $< 10^{-8}$ *Eh*) together with a Lebedev-434 grid (option Grid5) was used. Starting from the converged high-spin state, the other relevant states could easily be obtained with the FlipSpin option. The orbital occupation and spin density distribution was inspected in each case to verify convergence to the desired open-shell state.

X-ray Crystallographic Data Collection and Refinement of the Structures: Single crystals of **1** to **5** were coated with perfluoropolyether, picked up with a glass fiber, and mounted on a SMART APEX II CCD diffractometer equipped with a nitrogen cold stream operating at 171(2) K. Graphite monochromated Mo-K_α radiation (λ = 0.71069 Å) from a fine-focus sealed tube was used throughout. The crystallographic data of the compounds are listed in Tables 2 and 3. Cell constants were obtained from a least-squares fit of the diffraction angles of several thousand strong reflections. The data reduction was done with APEX2 v2.0,[46] while SIR-97[47] and SHELXL-97[48] were used for the structure solution and for the

Table 2. Summary of the crystal structure data collection and refinement for **1**, **2**, and **3**.

	1	**2**	**3**
F.w.	1464.23	1408.13	1485.17
Space group	triclinic $P\bar{1}$	triclinic $P\bar{1}$	triclinic $P\bar{1}$
a /Å	13.3011(12)	13.2564(7)	13.2357(18)
b /Å	15.8449(14)	16.0426(8)	16.2046(18)
c /Å	19.2444(16)	19.1440(10)	19.045(2)
α /°	109.917(6)	111.234(3)	110.725(8)
β /°	100.401(6)	99.343(3)	100.763(8)
γ /°	97.440(7)	99.224(3)	99.101(8)
V /Å^3	3669.7(6)	3636.8(3)	3639.6(8)
Z	2	2	2
T /K	171(2)	171(2)	171(2)
$\rho_{calcd.}$ /g cm^{-3}	1.325	1.286	1.355
μ(Mo-K_α) /cm^{-1}	0.487	0.595	0.803
Reflections collected	54979	41410	38581
Unique refl. [$I > 2\sigma(I)$]	17646/6407	17914/3943	5837/3289
No. parameters	879	876	916
Θ_{max} /°	28.11	28.34	19.00
$R^{[a]}$ [$I > 2\sigma(I)$]	0.069	0.094	0.090
$wR^{[a]}$ [$I > 2\sigma(I)$]	0.170	0.227	0.226

[a] $w = 1/[s^2(F_o^2) + (xP)^2]$ where $P = (F_o^2 + 2F_c^2)/3$, $x = 0.1063$ for **1**, $x = 0.1301$ for **2**, and $x = 0.1726$ for **3**.

Table 3. Summary of the crystal structure data collection and refinement for **4** and **5**.

	4	**5**
F.w.	1293.97	1351.94
Space group	triclinic $P\bar{1}$	triclinic $P\bar{1}$
a /Å	13.7472(9)	13.8477(10)
b /Å	14.6674(9)	14.9032(10)
c /Å	16.8493(10)	17.7119(12)
α /°	89.331(2)	100.662(4)
β /°	72.487(2)	110.746(4)
γ /°	65.617(2)	113.886(4)
V /Å^3	2926.08(41)	2885.74(133)
Z	2	2
T /K	171(2)	171(2)
$\rho_{calcd.}$ /g cm^{-3}	1.469	1.556
μ(Mo-K_α) /cm^{-1}	0.597	0.727
Reflections collected	30439	74022
Unique refl. [$I > 2\sigma(I)$]	12037/5614	13805/7692
No. parameters	731	775
Θ_{max} /°	26.45	28.13
$R^{[a]}$ [$I > 2\sigma(I)$]	0.058	0.048
$wR^{[a]}$ [$I > 2\sigma(I)$]	0.115	0.096

[a] $w = 1/[s^2(F_o^2) + (xP)^2]$ where $P = (F_o^2 + 2F_c^2)/3$, $x = 0.0521$ for **4**, and $x = 0.0466$ for **5**.

refinement, respectively. No absorption correction was employed. CCDC-699496, -699684, -699607, -699495, and -699494 (for structures **1**, **2**, **3**, **4**, and **5**, respectively) contain the supplementary crystallographic data for this paper. These data can be obtained free of charge from The Cambridge Crystallographic Data Centre via www.ccdc.cam.ac.uk/data_request/cif.

Supporting Information (see footnote on the first page of this article): ORTEP diagrams of **2** and **3** and the CW-X-band EPR spectrum of **2**.

Acknowledgments

U. S. thanks Prof. Dr. Nils Metzler-Nolte (Bochum) for generous access to the computational infrastructure of the institute. E. R. thanks Christopher Reinnig and Lars Müller (Mainz) for the ESI mass spectra.

[1] A. Caneschi, D. Gatteschi, P. Rey, *Prog. Inorg. Chem.* **1991**, *39*, 331–429.
[2] A. Caneschi, D. Gatteschi, R. Sessoli, P. Rey, *Acc. Chem. Res.* **1989**, *22*, 392–398.
[3] K. Inoue, H. Iwamura, *J. Am. Chem. Soc.* **1994**, *116*, 3173–3174.
[4] H. Iwamura, K. Inoue, T. Hayamizu, *Pure Appl. Chem.* **1996**, *68*, 243–252.
[5] A. Ito, Y. Nakano, M. Urabe, K. Tanaka, M. Shiro, *Eur. J. Inorg. Chem.* **2006**, 3359–3368.
[6] A. Alberola, E. Coronado, C. Gimenez-Saiz, C. J. Gomez-Garcia, F. M. Romero, A. Tarazon, *Eur. J. Inorg. Chem.* **2005**, 389–400.
[7] D. A. Shultz, S. H. Bodnar, K. E. Vostrikova, J. W. Kampf, *Inorg. Chem.* **2000**, *39*, 6091–6093.
[8] D. A. Shultz, K. E. Vostrikova, S. H. Bodnar, H. J. Koo, M. H. Whangbo, M. L. Kirk, E. C. Depperman, J. W. Kampf, *J. Am. Chem. Soc.* **2003**, *125*, 1607–1617.
[9] D. A. Shultz, R. M. Fico, S. H. Bodnar, R. K. Kumar, K. E. Vostrikova, J. W. Kampf, P. D. Boyle, *J. Am. Chem. Soc.* **2003**, *125*, 11761–11771.
[10] O. Kahn, R. Prins, J. Reedijk, J. S. Thompson, *Inorg. Chem.* **1987**, *26*, 3557–3561.
[11] C. G. Pierpont, C. W. Lange, *Prog. Inorg. Chem.* **1994**, *41*, 331–442.
[12] C. Benelli, D. Gatteschi, *Chem. Rev.* **2002**, *102*, 2369–2387.
[13] P. M. Allemand, G. Srdanov, F. Wudl, *J. Am. Chem. Soc.* **1990**, *112*, 9391–9392.
[14] R. G. Hicks, M. T. Lemaire, L. K. Thompson, T. M. Barclay, *J. Am. Chem. Soc.* **2000**, *122*, 8077–8078.
[15] T. M. Barclay, R. G. Hicks, M. T. Lemaire, L. K. Thompson, *Inorg. Chem.* **2003**, *42*, 2261–2267.
[16] B. D. Koivisto, R. G. Hicks, *Coord. Chem. Rev.* **2005**, *249*, 2612–2630.
[17] K. Awaga, T. Tanaka, T. Shirai, M. Fujimori, Y. Suzuki, H. Yoshikawa, W. Fujita, *Bull. Chem. Soc.* **2006**, *79*, 25–34.
[18] J. M. Rawson, F. Palacio, *(Pi)-Electron Magnetism from Molecules to Magnetic Materials*, **2001**, *100*, 93–128.
[19] A. Alberola, R. J. Less, C. M. Pask, J. M. Rawson, F. Palacio, P. Oliete, C. Paulsen, A. Yamaguchi, R. D. Farley, D. M. Murphy, *Angew. Chem. Int. Ed.* **2003**, *42*, 4782–4785.
[20] W. Fujita, K. Awaga, *J. Am. Chem. Soc.* **2001**, *123*, 3601–3602.
[21] M. T. Lemaire, *Pure Appl. Chem.* **2004**, *76*, 277–293.
[22] N. Ishii, Y. Okamura, S. Chiba, T. Nogami, T. Ishida, *J. Am. Chem. Soc.* **2008**, *130*, 24–25.
[23] R. Sessoli, *Angew. Chem. Int. Ed.* **2008**, *47*, 5508–5510.
[24] U. Schatzschneider, T. Weyhermüller, E. Rentschler, *Eur. J. Inorg. Chem.* **2001**, 2569–2586.
[25] N. Ito, S. E. V. Phillips, C. Stevens, Z. B. Ogel, M. J. Mcpherson, J. N. Keen, K. D. S. Yadav, P. F. Knowles, *Nature* **1991**, *350*, 87–90.
[26] F. Thomas, *Eur. J. Inorg. Chem.* **2007**, 2379–2404.
[27] J. A. Stubbe, W. A. van der Donk, *Chem. Rev.* **1998**, *98*, 2661–2661.
[28] D. S. Marlin, E. Bill, T. Weyhermüller, E. Rentschler, K. Wieghardt, *Angew. Chem. Int. Ed.* **2002**, *41*, 4775–4779.
[29] E. V. Gorelik, V. I. Ovcharenko, M. Baumgarten, *Eur. J. Inorg. Chem.* **2008**, 2837–2846.
[30] A. W. Addison, T. N. Rao, J. Reedijk, J. Vanrijn, G. C. Verschoor, *J. Chem. Soc., Dalton Trans.* **1984**, 1349–1356.
[31] N. C. Schiodt, F. F. deBiani, A. Caneschi, D. Gatteschi, *Inorg. Chim. Acta* **1996**, *248*, 139–146.
[32] U. Schatzschneider, T. Weyhermüller, E. Rentschler, *Inorg. Chim. Acta* **2002**, *337*, 122–130.
[33] A. Caneschi, D. Gatteschi, E. Rentschler, R. Sessoli, *Gazz. Chim. Ital.* **1995**, *125*, 283–286.
[34] P. J. Pessiki, S. V. Khangulov, D. M. Ho, G. C. Dismukes, *J. Am. Chem. Soc.* **1994**, *116*, 891–897.
[35] J. H. Van Vleck, *The Theory of Electric and Magnetic Susceptibilities*, Oup, London, **1932**.
[36] Olivier Kahn, *Molecular Magnetism*, VCH, New York, **1993**.
[37] Simulation of the experimental magnetic data with a full-matrix diagonalization of exchange coupling was performed with the julX program developed by E. Bill of the Max-Planck-Institute for Bioinorganic Chemistry.
[38] S. Stoll, A. Schweiger, *J. Magn. Reson.* **2006**, *178*, 42–55.
[39] S. Stoll, A. Schweiger, *Biol. Magn. Reson.* **2007**, *27*, 299–321.
[40] V. McKee, M. Zvagulis, J. V. Dagdigian, M. G. Patch, C. A. Reed, *J. Am. Chem. Soc.* **1984**, *106*, 4765–4772.
[41] D. R. Chapman, C. A. Reed, *Tetrahedron Lett.* **1988**, *29*, 3033–3036.
[42] C. Bätz, P. Amann, H. J. Deiseroth, L. Dulog, *Liebigs Ann. Chem.* **1994**, 739–740.
[43] F. Neese, *ORCA version 2.6.35*.
[44] A. Schafer, H. Horn, R. Ahlrichs, *J. Chem. Phys.* **1992**, *97*, 2571–2577.
[45] The Ahlrichs DZ basis set was obtained from the TurboMole basis set library under ftp.chemie.uni-karlsruhe.de/pub/basen.
[46] Bruker 2005 *APEX2 Software Suite version 2.0*.
[47] A. Altomare, M. C. Burla, M. Camalli, G. L. Cascarano, C. Giacovazzo, A. Guagliardi, A. G. G. Moliterni, G. Polidori, R. Spagna, *J. Appl. Crystallogr.* **1999**, *32*, 115–119.
[48] G. M. Sheldrick, *SHELXL-97*, *Program for Crystal Structure Refinement*, University of Göttingen, Germany, **1997**.

Received: December 24, 2008
Published Online: March 9, 2009

